

Cavity and background oscillations in Intrinsic Josephson Junctions

I. G. Hristov, R. D. Hristova and S. N. Dimova

Faculty of Mathematics and Informatics, St. Kliment Ohridski

University of Sofia, 5 James Bourchier Blvd., 1164 Sofia, Bulgaria,

emails: ivanh@fmi.uni-sofia.bg, radoslava@fmi.uni-sofia.bg, dimova@fmi.uni-sofia.bg

(Dated: November 10, 2015)

Starting with zero initial conditions we simulate the current-voltage characteristics (CVCs) of Intrinsic Josephson Junctions (IJJ) for parameters close to that of the BSCCO mesas. The simulation shows a regular pattern with voltage jumps at voltages satisfying the cavity resonance conditions. The calculated emission has peaks at every voltage jump. Analyzing the phases we observe a two-dimensional standing wave pattern with a kink configuration as their static part. Depending on the kink configuration and the bias current, the kink amplitudes may differ from π . By means of Fast Fourier Transform (FFT) we show that the frequencies excellently satisfy the ac Josephson relation as in the real experiments. Integer higher harmonics up to fifth order are also observed. Calculated amplitude maps for the frequencies achieved and their harmonics demonstrate that together with cavity modes there exist nonlinear background modes. Direct observation of the phase dynamics shows a relation between oscillations of the background modes and the static kink configuration: opposite static kinks in different junctions correspond to opposite (π -shifted) oscillations of the background modes.

PACS numbers: 74.50.+r, 74.72.-h, 85.25.Cp, 07.05.Tp

I. INTRODUCTION

The powerful THz radiation from BSCCO mesas at zero magnetic field being reported in 2007 [1] starts a new stage of intensive investigation of the Intrinsic Josephson Junctions (IJJ). A big progress has been made in mesa preparation technology, as a consequence self-heating effects and hot spot formations are significantly reduced [2]-[6]. The last progress gives possibility to increase the number of junctions in mesas from ≈ 500 [1] to ≈ 3000 [4], the radiation power from $\approx 0.5\mu W$ [1] to $\approx 30\mu W$ [2] and the frequency from $\approx 0.85THz$ [1] up to $\approx 2.4THz$ [6].

Still, the mechanism of powerful radiation has not been fully explained. It has been generally accepted that high radiation power could be achieved when the frequency ω satisfies the resonance condition:

$$\omega = \omega_J = \omega_{cav}. \quad (1)$$

This means that ω satisfies the ac Josephson relation $\omega = \omega_J = 2ev/\hbar$ and it simultaneously coincides with some cavity mode frequency: $\omega = \omega_{cav}$. Here e is the electric charge, \hbar is Planck's constant and v is the applied dc voltage. Cavity mode frequency ω_{cav} depends on mesa geometry and dimensions [7]. The resonance condition (1) is rather restrictive and usually it is not exactly observed in the real experiments. Although the ac Josephson relation is always excellently fulfilled in the experiments, it is not yet explained why the frequency ω may differ from the corresponding cavity mode frequency ω_{cav} [4],[5]. The observed "dual" source mechanism in experimental works [8], [9] is confirmed numerically in [10] but it's still not well understood.

There are two main concepts for the powerful radiation mechanism - the coupling to the resonance modes is

obtained by π kinks [11],[12] or by breather type self oscillation (not necessarily with π amplitude) [13]. It is important to mention that there is a difference in the mathematical models used in [11] and [13]. Periodic boundary conditions in z-direction (stacking direction) are posed in [11] while the boundary conditions in [13] are nonperiodic. Although the parameters are almost the same, there is a difference in the characteristic mode velocities [14]. Particularly the maximum (in-phase) plasma velocities significantly differ for usual simulations with about 10-20 junctions. On the other hand the use of nonperiodic boundary conditions in [13] makes the junctions to be not identical, the amplitudes of oscillations in the external junctions lower than these in the internal ones and hence the picture becomes more complicated. Actually, it is reasonable to think that the solutions in [11] and [13] are generally of the same type and not to treat them as different.

In addition we want to note the new state with coexisting moving fluxons and longitudinal plasma wave in [15]. This state may be also important for the future understanding of powerful THz radiation.

In this work we carry out numerical simulation by solving a system of 1D Sine-Gordon equations which describe well the rectangular mesas in which the zero mode is realized in y-direction. Because in reality the number of junctions is thousands, we prefer to use periodic boundary conditions as in [11]. We achieve kinks in the numerical simulations and perform a detailed analysis of their possible amplitudes. We show that the kink amplitudes may differ from π , they depend on the kink configuration in z-direction and on the bias current. A crucial observation is the alternative character of the static kink configuration and approximately the same number of kinks and anti-kinks in the stack. We show by FFT analysis that radiation frequencies excellently satisfy the ac Joseph-

son relation as in the real experiments. Calculated amplitude maps and the direct phase analysis show simultaneous existence of nonlinear background modes. Although the background modes are hard to see at the top of the current steps, corresponding to a particular cavity mode excitation [11], their amplitudes become higher when the current decreases. The background modes are very well seen at the bottom of the current steps. There is a strong relation between the oscillations of the background modes and the static kink configuration: the opposite static kink chains in the different junctions correspond to opposite (π -shifted) oscillations of the background modes.

II. MATHEMATICAL MODEL

Assuming zero mode along y-axis we consider a system of 1D Sine-Gordon equations (xz -model) [16]. For stack of N periodically stacked junctions with length L the column vector $\varphi = (\varphi_1, \dots, \varphi_N)^T$ of the gauge invariant phase differences satisfies the standard inductive model [17]:

$$S(\varphi_{tt} + \alpha\varphi_t + \sin\varphi - \gamma) = \varphi_{xx}, \quad 0 < x < L. \quad (2)$$

Here S is the $N \times N$ matrix

$$S = \begin{pmatrix} 1 & s & 0 & \dots & 0 & s \\ s & 1 & s & 0 & \dots & 0 \\ \vdots & \vdots & \vdots & \vdots & \vdots & \vdots \\ 0 & \dots & 0 & s & 1 & s \\ s & \dots & 0 & 0 & s & 1 \end{pmatrix}$$

with $s = -\lambda/(w \sinh(d/\lambda) + 2\lambda \cosh(d/\lambda))$ being the inductive coupling parameter, λ is the London penetration depth, w is the thickness of insulators, d - the thickness of superconductors.

In (2) $\alpha = \sqrt{\hbar/2ej_c C R^2}$ is the damping parameter, where R, C, j_c are the normal resistance, the capacitance and the critical current per unit length respectively. The applied bias current γ is normalized to the critical current j_c . The space x in (2) is normalized to the Josephson penetration depth $\lambda_J = \sqrt{\hbar/2e\mu_0 j_c t'}$, the time t to the inverse of plasma frequency $\omega_{pl} = \sqrt{\hbar C/2ej_c}$, where t' is the effective magnetic thickness of the barrier, μ_0 is the magnetic constant. In calculated further current-voltage characteristics (CVCs) the voltage V will be normalized to $\hbar\omega_{pl}/2e$. The voltage V in the stack is the sum of voltages v_i in the junctions: $V = \sum_{i=1}^N v_i$. When v_i are equal as a result of using periodic conditions for the stack, we will write simply v .

Together with equation (2) we consider radiative boundary conditions [18],[19]:

$$\varphi_x(x=0, L) = \pm \frac{1}{\tilde{Z}}(\varphi_t(x=0, L) - \langle \varphi_t \rangle). \quad (3)$$

With $\langle \cdot \rangle$ we denote the instant spatial average, plus sign corresponds to the left edge of the stack ($x=0$), minus sign - to the right edge ($x=L$). \tilde{Z} is the normalized impedance. For $\tilde{Z} = \infty$ boundary conditions (3) become simple Neumann conditions:

$$\varphi_x(x=0, L) = 0. \quad (4)$$

Because \tilde{Z} is huge in reality [13] and also it is not easy to implement (3), most authors prefer to use Neumann conditions for their simulations. In our simulations we use the boundary conditions (3).

III. CAVITY MODE FREQUENCIES AND THE COUPLING PARAMETER

For rectangular mesas described by the xz -model, the frequencies for the cavity modes $m, m=1, 2, 3, \dots$ (in normalized units) are given by [20]:

$$\omega_{cav}^m = \frac{mC_{max}}{2L} \quad (5)$$

Here C_{max} is the maximum plasma velocity. $C_{max} = 1/\sqrt{\lambda_{min}(S)} = 1/\sqrt{(1+2s)}$, where $\lambda_{min}(S)$ is the minimal eigenvalue of the cyclic tridiagonal matrix S and does not depend on N . For the usual (not cyclic) tridiagonal matrix $\lambda_{min} = 1/\sqrt{(1+2s \cos(\pi/(N+1)))}$ [13].

In our simulations we take s close to $s = -0.5$, which corresponds to strong inductive coupling (as for BSCCO crystals). It is important to note again the difference between using models with cyclic and not cyclic matrix. As an example for $s = -0.49985, N = 12$, C_{max} for the cyclic and not cyclic matrix are respectively 57.7 and 5.83, and the condition numbers of the matrices are respectively 6665 and 67.1. For $s = -0.499995$, which is usually used in simulations [21], C_{max} changes to 316 and 5.87 respectively and the condition numbers to 2.10^5 and 67.8. The above difference in wave velocities nicely explains the different results in [11],[13] and the achieved higher modes in [13] - up to 12. Moreover, it is difficult to determine parameter s rigorously [22]. For all the above reasons (the use of periodic boundary conditions, numerical accuracy, not strictly determined s in reality), we take s phenomenologically. The results that follow are achieved for $s = -0.49985$.

IV. RESULTS

We solve problem (2),(3) by using a leap-frog difference scheme. The nonstandard boundary conditions (3) are approximated by the method of balance [23], which provides energy conservation of the numerical scheme. Simulations are made for $N = 12, L = 30, s = -0.49985, \alpha = 0.05, 0.07, 0.13, \tilde{Z} = 6.10^5$. The bias current γ is taken with noise of amplitude 10^{-8} .

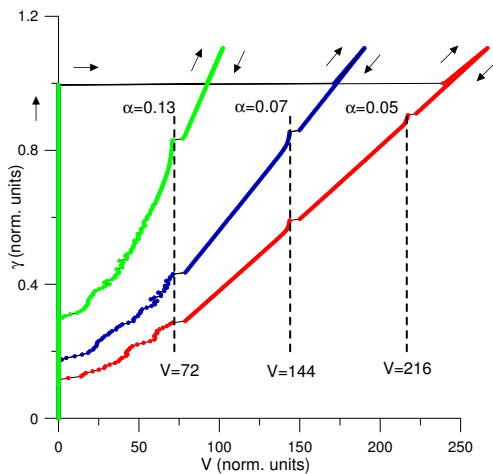


FIG. 1. Simulated CVC's for different dissipation parameters.

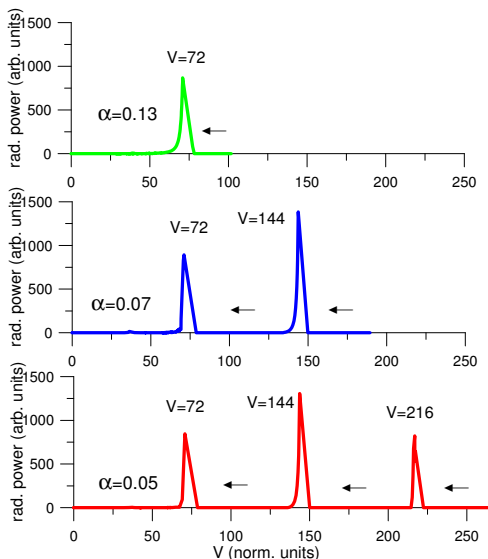


FIG. 2. Emission power corresponding to CVC's calculated by the Poynting vector at the edge $x = 0$.

We don't use any special initial conditions. We use zero initial conditions at the start of our simulations. A typical simulation of the outermost branch of the CVC works as follows. Starting with zero initial conditions at $\gamma = 0$ we increase γ by steps of 0.005 until (at $\gamma = 1.0$) all the junctions switch to resistive state. We continue increasing γ up to 1.1 and then start to decrease γ . A hysteresis region, typical for IJJ, is observed, i.e. at the decreasing part of CVC, the voltage V remains nonzero for $\gamma < 1$ until all the junctions switch to superconductive state ($V = 0$) at some bias current.

CVCs for $\alpha = 0.05, 0.07, 0.13$ are shown in Fig.1. Different α model different mesa temperatures [13]. CVCs show a nice regular pattern. Depending on the possible achievable voltage V , jumps are observed at $V \approx 72$, $V \approx 144 = 2 \times 72$, $V \approx 216 = 3 \times 72$. Voltage $V \approx 72$ in the stack corresponds to voltage $v \approx 6$ per junction.

Radiation power achieved by calculating time average of the Poynting vector [24] at the edge $x = 0$ of the stack is shown in Fig.2. Each voltage jump corresponds to a peak in the radiation power. These voltage jumps are different from the jumps to another voltage branch such as those in the experimental results in [1], where different groups of junctions are involved in resonance. In our case we remain on the same (outermost) branch.

Direct analysis of the calculated φ -dynamics shows that the peaks at $V \approx 72, 144, 216$ correspond to an excitation of the cavity modes 1, 2, 3 respectively [20]. The phase in a particular junction is a sum of three terms: the linear term vt , a static kink term (time independent) and an oscillating term [11]. A clear two-dimensional standing wave pattern is seen as in [11],[13], where the oscillating term of the phases φ is approximately uniform in z-direction and satisfies the linear wave equation:

$$\varphi_{tt} = (C_{max})^2 \varphi_{xx} \quad (6)$$

with Neumann boundary conditions, except at the bottom of the current steps. As our numerical simulations show there exist a small nonuniform oscillating part with the same frequency, which is clearly seen at the bottom of the current steps. Unlike the cavity mode part this part has a nonlinear origin. We use the terminology from [10] and call this oscillating mode a background mode. We will return to describe the background modes later.

It is worth to note that the cavity mode 1 excitation is more stable for larger dissipation parameter α . This is clearly seen from the loosing of smoothness of CVC around the resonance voltage for $\alpha = 0.05, 0.07$ (Fig. 1) and also from the direct observation of the phase φ which shows a very complicated picture, hard to analyze. This is in a good agreement with the experimental results in [4],[5] where the highest power for cavity mode 1 is achieved for relatively higher temperatures.

A. Static kink configurations

The static part of φ consists of some configuration of chains of kinks (k) and anti-kinks (a) in every junction as in [11],[12]. A crucial observation is the alternative character of the static kink configuration, i.e. alternating of opposite kinks (kinks and anti-kinks) in x and z-direction. As numerous simulations show the number of kinks and antikinks in the stack is usually one and the same; if it is not, the difference is at most 2. For mode m the chains consist of m kinks or antikinks, for example $\underbrace{akkaak...ak}_m$. A kink configuration in the stack is a sequence of chains starting with the first junction. For example in the case of excitation of third cavity mode the sequence $(aka, kak, aka, ...)$ corresponds to a configuration with chain aka in the first junction, kak in the second and so on.

We analyze now in detail some kink configurations observed when cavity mode 2 is excited. They are achieved

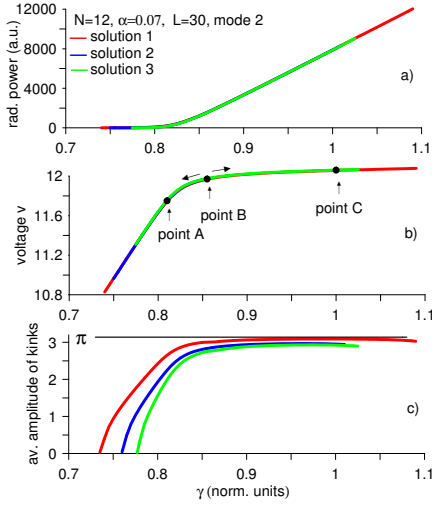


FIG. 3. Kink amplitudes, current-voltage branches and emission powers for different kink configurations corresponding to excitation of cavity mode 2.

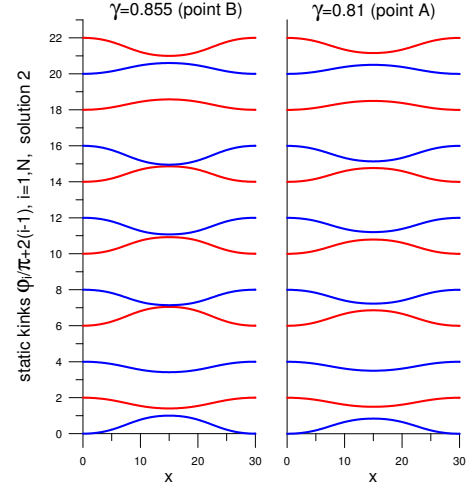


FIG. 4. Static kink configuration at points A and B for solution 2.

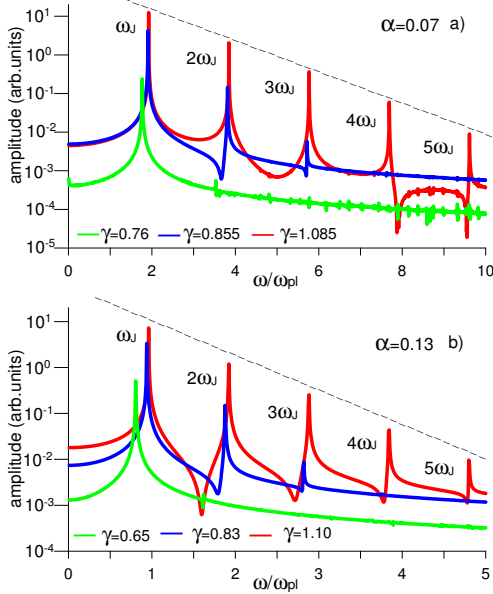


FIG. 5. FFT of the electric field φ_t at the edge $x = 0$ of the stack for different bias points on the current steps of cavity mode 2 (a) and cavity mode 1 (b).

at $N = 12, L = 30, s = -0.49985, \alpha = 0.07$. The picture for cavity mode 1, achieved at $N = 12, L = 30, s = -0.49985, \alpha = 0.13$ and for mode 2 at different α is similar. Regardless the static kink configuration for numerous repeated simulations, cavity mode 2 is excited always when $\gamma = 0.855$ at the decreasing part of CVC. The results for the radiation power, the voltages and the kink amplitudes, corresponding to three different kink configurations (three solutions), are shown in Fig.3. All the curves in Fig.3 are obtained by reversing γ at point B ($\gamma = 0.855$), i.e. increasing γ until the correspond-

ing solution exists. Figure 3b actually shows the current steps in the CVC corresponding to the excitation of cavity mode 2 with different kink configurations. The heights of the current steps differ for different configurations. Solution 1 corresponds to the kink configuration $(ka, ak, ka, ak, ka, ak, ka, ak, ka, ak, ka, ak)$, solution 2 - to $(ka, ak, ak, ka, ak, ka, ak, ka, ak, ka, ka, ak)$, solution 3 - to $(ka, ak, ak, ka, ka, ak, ak, ka, ak, ka, ka, ak)$. The total number of kinks and antikinks for the above kink configurations is one and the same. From the top to the bottom of the current steps the kink amplitudes decrease from almost π to zero. Solution 1 exists at largest range in γ and can achieve maximal radiation power (Fig.3a). Although for every coexisting point the voltages and the power are approximately the same for solutions 1, 2, 3, the kink amplitudes are not. The average in the stack kink amplitudes are shown in Fig.3c. The average kink amplitude is greatest for Solution 1 for every γ . The maximal average kink amplitude is close (≈ 3.10), but less than π . Decreasing γ from point B the kink amplitudes strongly decrease together with decreasing the voltage and the radiation power. Kink configuration for solution 2 at point A ($\gamma = 0.81$) and point B ($\gamma = 0.855$) in Fig.4 confirm the last conclusion. It is worth to note that although the average kink amplitude is always less than π , it could be even greater than π for particular junction and depending on the kink configuration. For example the kink amplitude in junction 9 for solution 3 at point C ($\gamma = 1.0$) is 3.2631.

B. Fast Fourier Transform analysis and observation of oscillating background modes

To analyze the radiation frequency we have used Fast Fourier Transform (FFT) of the electric field φ_t with res-

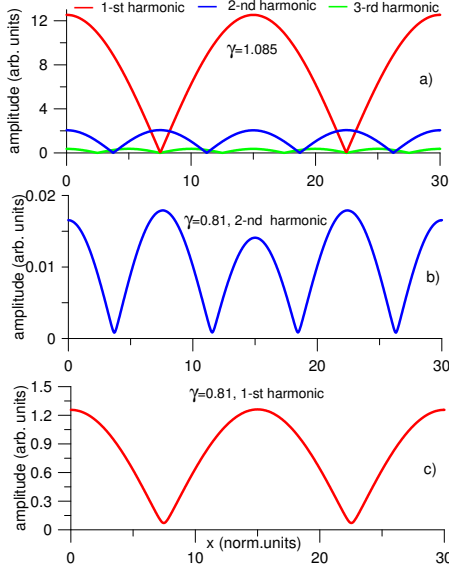


FIG. 6. Amplitude maps of the electric field at different bias currents: At the top of the current step (a) the amplitudes for the first three harmonics excellently fit to the cavity amplitudes. At the bottom of the current step (b,c) the amplitudes deviates from those corresponding to the cavity modes.

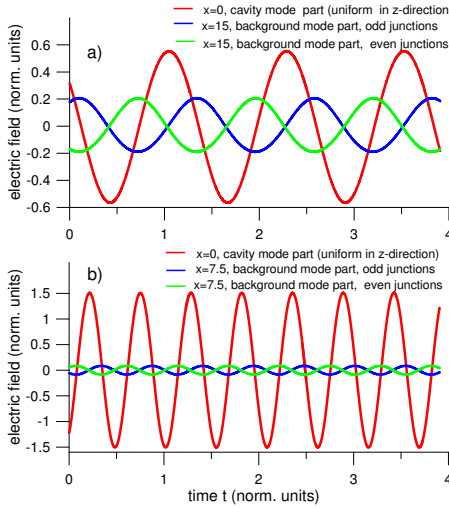


FIG. 7. Oscillations of the cavity mode part and the background mode part of the electric field for the excited cavity mode 1 (a) and cavity mode 2 (b). The shift between the oscillations of the background and the cavity mode is close to $\pi/2$. The oscillations of the background mode in the adjacent junctions are anti-phase (π -shifted).

olution $2^{-7}\omega_{pl}$. Calculated by FFT radiation frequency ω excellently fulfills the ac Josephson relation, which in normalized units is $\omega = \omega_J = v/2\pi$. The FFT results for the oscillation of the electric field φ_t at the edge $x = 0$ of the stack are shown in Fig.5a (cavity mode 2) and Fig.5b (cavity mode 1). The oscillation amplitudes decrease together with the decreasing bias current γ (decreasing ra-

diation power). Integer higher harmonics up to the fifth order are also visible on the top of the current steps but their number decrease with γ and completely disappear at the bottom of the current steps. At the top of the current steps the amplitudes decrease exponentially as it is seen from dashed lines in Fig.5. Integer higher harmonics are obtained in many experiments, for example in: [6],[8],[9],[25], where an exponential rate of decreasing of harmonics amplitudes is also observed.

To check the resonance condition (1) we calculate ω_J from calculated voltage at the top of the current step of cavity mode 2 and ω_{cav}^2 from formula (5). They differ by less than 10^{-5} : $\omega_J = \omega_{cav}^2 = 1.9245$. Although the voltage v is in a pretty large range for kink solutions ($v \in (10.8, 12)$ in Fig. 3b), the frequency tunability for powers greater than 10% and 5% of the maximal power is only about 1% and 2% respectively. The fact that the frequency at the maximal achieved power excellently fits with the cavity frequency agrees with the experimental results [2]-[4]. On the other hand the frequency tunability around the cavity frequency is much larger in the experiments than in our simulation. In our opinion this is due to the fact that the considered model doesn't treat the temperature inhomogeneities which exist in reality.

In order to understand whether the oscillating part consists only of cavity mode oscillations, we calculate the amplitude maps of the electric field, i.e. we calculate the amplitude for every harmonic frequency by using FFT for every point $x \in [0, L]$. It is correct because although the amplitudes slightly depend on the output bins, the frequencies are the same for every x . Figure 6a shows the amplitudes of the first three frequency harmonics corresponding to the top of the current step of the excited cavity mode 2. In our case the second and the third harmonics are the cavity modes 4 and 6 respectively. The amplitudes excellently fit with the properly scaled $|\cos|$ -function: $|\cos(2\pi x/L)|$, $|\cos(4\pi x/L)|$, $|\cos(6\pi x/L)|$. On the other hand at the bottom of the current step (Fig.6b,c) the amplitudes deviate from those corresponding to the cavity modes, particularly they are far from zero at the nodes of the cavity modes. This result confirms the existence of oscillating background modes. Although it is hard to detect background mode oscillations at the top of the current steps, we suppose that they support the cavity mode oscillations at the entire current step. The background modes have a nonlinear origin. Direct analysis shows that they are strongly related with the static kink configurations: opposite static kink chains in different junctions correspond to opposite (π -shifted) oscillations of the background modes. In our case the opposite static kink chains for the cavity mode 1 are a and k , for the cavity mode 2 they are ak and ka .

The oscillations of the background modes in the adjacent junctions (odd and even) for excited cavity mode 1 at $\gamma = 0.65$, $\alpha = 0.13$ are shown in Fig.7a. The static kink configuration is $(k, a, k, a, k, a, k, a, k, a, k, a)$. The background oscillations in the odd and the even junctions are anti-phase (π -shifted to one another). The shift with

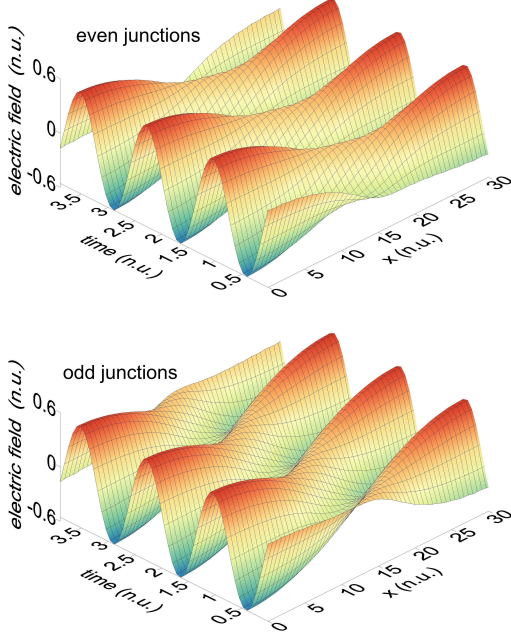


FIG. 8. Time evolution of the electric field φ_t at the bottom of the current step corresponding to an excitation of cavity mode 1. Parameters are $\alpha = 0.13$, $\gamma = 0.65$. The existence of the background mode is visible.

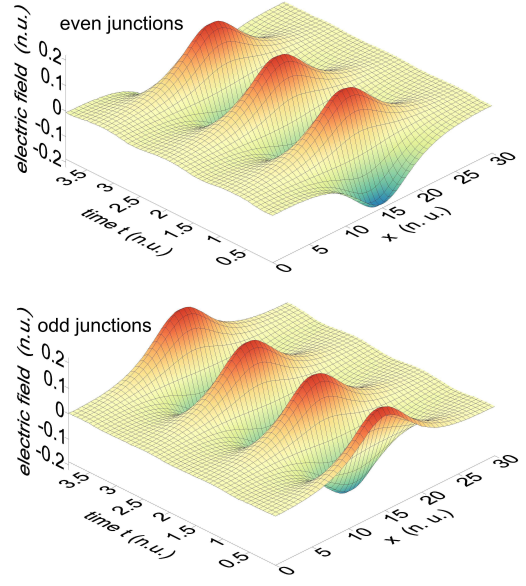


FIG. 9. Time evolution of the background mode part of the electric field (the electric field φ_t with subtracted cavity mode part). Parameters are $\alpha = 0.13$, $\gamma = 0.65$. Oscillations in adjacent junctions are anti-phase (π -shifted).

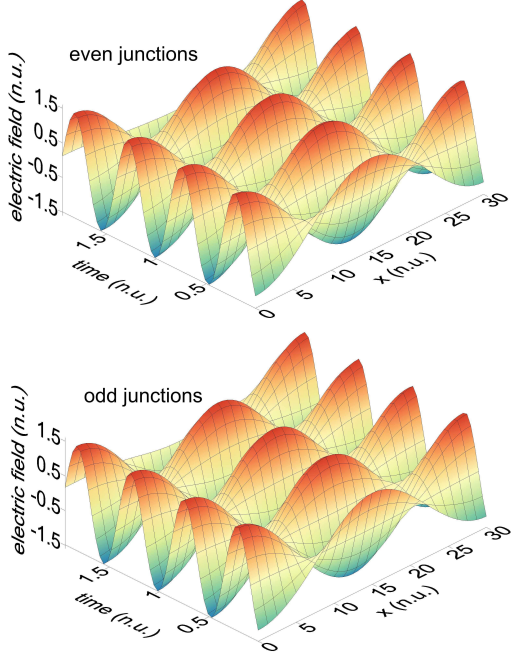


FIG. 10. Time evolution of the electric field φ_t at the bottom of the current step corresponding to an excitation of cavity mode 2. Parameters are $\alpha = 0.07$, $\gamma = 0.81$. The existence of the background mode is not clearly visible because its amplitude is relatively small.

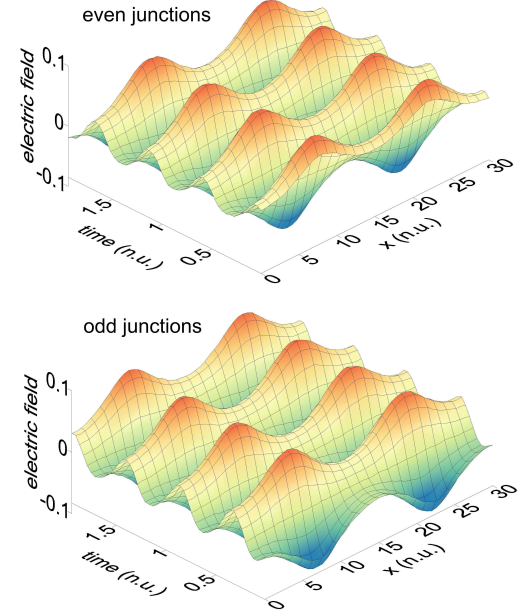


FIG. 11. Time evolution of the background mode part of the electric field (the electric field φ_t with subtracted cavity mode part and its second harmonic). Parameters are $\alpha = 0.07$, $\gamma = 0.81$. Oscillations in adjacent junctions are anti-phase (π -shifted).

respect to the cavity mode oscillation slightly deviates from $\pi/2$. The time evolution of the electric field and the electric field with subtracted cavity mode part are shown in Fig.8 and Fig.9 respectively. As it is seen from these figures, the amplitudes of the background modes are not uniform, but they are higher at the centers of the kinks.

The oscillations of the background modes in the adjacent junctions (odd and even) for excited cavity mode 2 at $\gamma = 0.81$, $\alpha = 0.07$ are shown in Fig.7b. The static kink configuration is $(ka, ak, ka, ak, ka, ak, ka, ak, ka, ak, ka, ak)$ (solution 1). Here the background amplitudes are relatively smaller because we are not at the very bottom of the current step. The picture is similar, the anti-phase background oscillations are clearly seen in Fig. 7b. The shift with respect to the cavity mode oscillation is very close to $\pi/2$. The time evolution of the electric field and the electric field with subtracted first and second cavity harmonics are shown in Fig.10 and Fig.11 respectively. Background mode oscillations are again nonuniform, but higher at the centers of the kinks. Let us note that if we consider kink configuration $(ka, ak, ak, ka, ak, ka, ak, ka, ak, ka, ka, ak)$ (solution 2), the background oscillations are not anti-phase in the adjacent junctions (odd and even), but they are anti-phase in the following groups of junctions: $\{1,4,6,8,10,11\}$ and $\{2,3,5,7,9,12\}$.

V. CONCLUSIONS

By means of numerical simulations we show that the coupling to the resonance modes is obtained by a static kink configuration in z-direction. The kink amplitudes may differ from π depending on the kink configuration and the point on the current step. The kink configurations have alternative character with approximately equal number of kinks and anti-kinks. Calculated amplitude maps for the radiation frequencies and direct phase observation show the existence of nonlinear background modes together with the cavity modes, thus contributing to the improvement of the mechanism for powerful THz radiation in IJJs at zero magnetic field. A relation between the oscillations of the background modes and the static kink configuration is established: opposite static kink chains in different junctions correspond to opposite (π -shifted) oscillations of the background modes.

Acknowledgments

We thank Prof. D.Sc. Shukrinov and Dr. Rahmonov for valuable discussions and important remarks. This work is supported by the National Science Fund of BMSE under grant I-02/9/2014 and by the Sofia University Science Fund under grant N75/2015. We thank for the opportunity to use the computational resources of ICT-BAS.

-
- [1] L. Ozyuzer, A. E. Koshelev, C. Kurter, N. Gopalsami, Q. Li, M. Tachiki, K. Kadowaki, T. Yamamoto, H. Minami, H. Yamaguchi, et al., *Science* **318**, 1291 (2007).
 - [2] S. Sekimoto, C. Watanabe, H. Minami, T. Yamamoto, T. Kashiwagi, R. A. Klemm, and K. Kadowaki, *Appl. Phys. Lett.* **103**, 182601 (2013).
 - [3] M. Ji, J. Yuan, B. Gross, F. Rudau, D. Y. An, M. Y. Li, X. J. Zhou, et al., *Appl. Phys. Lett.* **105**, 122602 (2014).
 - [4] T. Kitamura, T. Kashiwagi, T. Yamamoto, M. Tsujimoto, et al., *Appl. Phys. Lett.* **105**, 202603 (2014).
 - [5] T. Kashiwagi, T. Yamamoto, T. Kitamura, K. Asanuma, C. Watanabe, K. Nakade et al., *Appl. Phys. Lett.* **106**, 092601 (2015).
 - [6] T. Kashiwagi, K. Sakamoto, H. Kubo et al., *Appl. Phys. Lett.* **107**, 082601 (2015).
 - [7] R. Klemm and K. Kadowaki, *J. Phys.: Condens. Matter* **22**, 375701 (2010).
 - [8] M. Tsujimoto, K. Yamaki, K. Deguchi, T. Yamamoto, et al., *Phys. Rev. Lett.* **105**, 037005 (2010).
 - [9] K. Kadowaki et al., *J. Phys. Soc. Jpn.* **79**, 023703 (2010).
 - [10] H. Asai, M. Tachiki, and K. Kadowaki, *Phys. Rev. B* **85**, 064521 (2012).
 - [11] S. Lin and X. Hu, *Phys. Rev. Lett.* **100**, 247006 (2008).
 - [12] X. Hu and S. Z. Lin, *Phys. Rev. B* **80**, 064516 (2009).
 - [13] V. M. Krasnov, *Phys. Rev. B* **83**, 174517 (2011).
 - [14] R. Kleiner, *Phys. Rev. B* **50**, 6919 (1994).
 - [15] I. Rahmonov, Y. Shukrinov, and A. Irie, *JETP letters* **99**, 632 (2014).
 - [16] S. Lin and X. Hu, *Phys. Rev. B* **86**, 054506 (2012).
 - [17] S. Sakai, P. Bodin, and N.F. Pedersen, *J. Appl. Phys* **73**, 2411 (1993).
 - [18] S. Lin, X. Hu, M. Tachiki, *Phys. Rev. B* **77**, 014507 (2008).
 - [19] V. Krasnov, *Phys. Rev. B* **82**, 0134524 (2010).
 - [20] T. Kashiwagi, M. Tsujimoto, T. Yamamoto, H. Minami, et al., *J. J. Appl. Phys.* **51**, 010113 (2012).
 - [21] R. Kleiner, T. Gaber, and G. Hechtfisher, *Phys. Rev. B* **62**, 4086 (2000).
 - [22] H. B. Wang, S. Guenon J. Yuan, A. Iishi, S. Arisawa, et al., *Phys. Rev. Lett.* **102**, 017006 (2009).
 - [23] A. Samarskii, *The theory of difference schemes*, Vol. **240**, CRC Press, (2001).
 - [24] H. Matsumoto, T. Koyama, M. Machida, M. Tachiki, *Physica C* **468**, 1899 (2008).
 - [25] K. Kadowaki, et al., *Physica C* **468**, 634 (2008).